INTERNATIONAL SOCIETY FOR SOIL MECHANICS AND GEOTECHNICAL ENGINEERING

SIMSG ISSMGE

Prediction of the Behaviour of Expansive Soils

Maki Ito
University of Regina, Regina, Saskatchewan, Canada
Yafei Hu
Centre for Sustainable Infrastructure Research Institute for Research in Construction National Research Council Canada, Regina, Saskatchewan, Canada

ABSTRACT
Water content and matric suction in unsaturated soils change due to infiltration and evaporation. For soils such as expansive clays, this results in soil volume changes and consequent ground movement. In general, the movement is uneven and induces stresses on civil infrastructure built in and on expansive soils. In some cases, the stresses are great enough to cause infrastructure failure. This paper summarizes information about predicting the displacement behaviour of clay soils. The prediction was made from a coupled, two-dimensional soil-atmosphere model. The resulting matric suctions were used as the initial condition for a displacement model used to predict vertical displacements in the soil. The soil suction and water content fluctuated widely close to the ground surface and the effect reduced gradually with depth. From the soil displacement model, wind speed, net radiation, precipitation, and park watering were found to be major contributors to the changes in matric suction and, consequently, soil displacements close to the ground surface.

RÉSUMÉ
La teneur en eau et l'aspiration matriciel dans les sols non saturés change en raison de l'infiltration et l'évaporation. Pour les sols tels que les argiles gonflantes, cela se traduit par des changements de volume du sol et le mouvement du sol conséquente. En général, le mouvement est inégal et induit des contraintes sur les infrastructures civiles construites dans et sur les sols gonflants. Dans certains cas, les contraintes sont assez grandes pour causer une défaillance de l'infrastructure. Ce document résume l'information sur la prédiction du comportement de déplacement des sols argileux. La prédiction a été faite à partir d'un couplage, en deux dimensions du modèle sol-atmosphère. Les aspirations résultant matricielles ont été utilisés comme condition initiale pour un modèle de déplacement utilisé pour prédire les déplacements verticaux dans le sol. La succion du sol et de teneur en eau largement fluctué près de la surface du sol et l'effet de réduire progressivement avec la profondeur. Du modèle de déplacement du sol, la vitesse du vent, le rayonnement net, la précipitation, et l'arrosage du parc ont été trouvés à être des contributeurs majeurs aux changements dans l'aspiration matricielle et, par conséquent, les déplacements du sol près de la surface du sol.

1   INTRODUCTION

Civil infrastructure built in or on expansive clay may experience severe damages due to the swelling and shrinking properties of the soils. Expansive soils swell/shrink as a result of change in soil water content. The soil water content is governed by the infiltration entering the soil due to precipitation and exfiltration leaving the soil due to evaporation at times when the ground is not frozen. This soil-moisture interaction is dependent on local climate. In arid and semi-arid climate zones, the net moisture loss through evaporation usually exceeds the moisture gain through annual precipitation. For expansive clay in these zones, the rate of evaporation significantly influences soil shrinkage, which in turn, affects subsequent moisture intake, leading to the significant volume change.

Modeling the in/exfiltration flux was developed based on the conservation of mass theory. Wilson et al. (1994) developed a coupled soil-atmosphere model for evaporation flux from the soil surface. A column of ideal, cohesionless, uniform sand was first used in the laboratory to validate the model. The model was subsequently adapted to suit various types of soils (Wilson et al., 1997). From this, it was found that a relationship existed between the evaporation rate and the soil suction because the vapour pressure gradient between the soil surface and the ambient atmosphere governed the evaporation flux from a soil surface.

Gitirana (2006) modified the Penman method (1948), which was originally developed for estimating the potential evaporation from open water and was adapted to estimate the potential evaporation from unsaturated soil surfaces. The estimated fluxes can be used as a boundary condition of soil-atmosphere analysis to evaluate the atmosphere interactions with soils.

The volume change properties of unsaturated expansive soils are governed by the two independent stress variables such as net normal stress, $(\sigma - u_a)$ and matric suction, $(u_a - u_w)$, where σ is net total stress, u_a is pore-air pressure, and u_w is pore-water pressure (Fredlund and Morgenstern, 1977). From this knowledge, the suction changes due to ambient weather conditions can be used as initial and final conditions to predict soil displacement.

The main objective of this work was to simulate soil displacement based on the suction data predicted from the soil-atmosphere coupled model based on one year of local climate data.
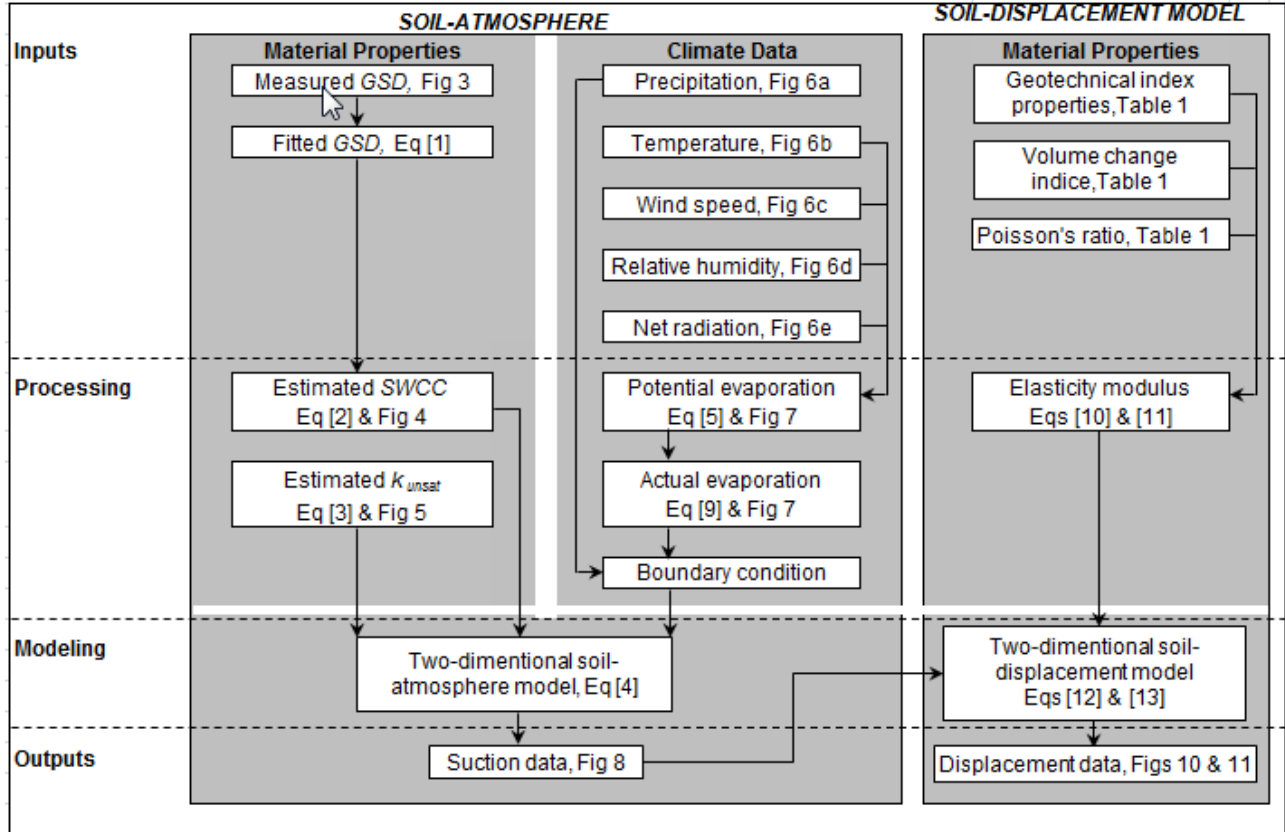
Figure 1. Modeling process

2 MODELLING PROCESS

Figure 1 describes the uncoupled soil-atmosphere/soil-displacement modeling process. First, a two-dimensional soil-atmosphere model requires two input categories: soil properties and atmospheric parameters. The soil properties consisted of a soil water characteristic curve (SWCC) and a hydraulic conductivity function. The SWCC was estimated by using SoilVision software based on index properties determined in the laboratory, including water content (w), specific gravity (G_s), dry unit weight (γ_d), and a grain size distribution (GSD) curve. Similarly, the hydraulic conductivity function was estimated from a saturated hydraulic conductivity (k_{sat}) and the estimated SWCC. The climate data provided the infiltration and exfiltration fluxes to determine the boundary condition and then the net flux was calculated in relation to soil properties. The model calculated matric suction as a function of time and depth. Second, vertical soil displacement was predicted with respect to changes in matric suction. The elasticity parameters were calculated from the volume change indices obtained in a consolidation test performed previously on Regina clay (Vu, et al., 2007). The Poisson's ratio was estimated from the typical values of similar soils.

3 GOVERNING EQUATIONS

3.1 Material Properties

The SWCC was estimated from measured index properties (w, Gs, and γ_d) and GSD. The GSD curve was fitted by the following Pedo-Transfer Function, $P_p(d)$, (Fredlund et al., 2002):

$$P_p(d) = \frac{1}{\ln\left[\exp(1)+\left(\frac{a_{gr}}{d}\right)^{n_{gr}}\right]^{m_{bi}}}\left\{1-\left[\frac{\ln\left(1+\frac{d_r}{d}\right)}{\ln\left(1+\frac{d_r}{d_m}\right)}\right]^7\right\} \qquad [1]$$

where, a_{gr}, n_{gr}, m_{bi}, and d_r are fitting parameters for the initial break point of the curve, the steepest slope of the curve, the shape of the fines part of the curve, and the amount of fines in soil, respectively; and d and d_m are grain sizes under consideration and the minimum allowable, respectively.

The fitted GSD curve was divided into smaller groups of nearly same size grains and a unique SWCC was obtained for each group using the following equation (Fredlund and Xing, 1994):

$$w_w = w_s\left[1-\frac{\ln\left(1+\frac{\psi}{h_r}\right)}{\ln\left(1+\frac{10^6}{h_r}\right)}\right]\left[\frac{1}{\left\{\ln\left[\exp(1)+\left(\frac{\psi}{a_f}\right)^{n_f}\right]\right\}^{m_f}}\right] \qquad [2]$$

where w_w and w_s are gravimetric water content and saturated gravimetric water content, respectively; a_f, n_f, m_f, and h_r are fitting parameters for the air entry value, soil desaturation rate, function curvature at high suction, and soil suction (ψ) at the residual water content, respectively.

The sum of the *SWCC* segments generated the entire *SWCC* that, along with the saturated hydraulic conductivity (k_{sat}) was used to determine the unsaturated hydraulic conductivity function ($k_r(\psi)$) (Fredlund, 2004):

$$k_r(\psi) = (k_s - k_{min})\left[\left[1 - \frac{ln(1+\frac{\varphi}{h_r})}{ln(1+\frac{10^6}{h_r})}\right]\left[\frac{1}{ln\left[exp(1) + (\frac{\varphi}{a_f})^{n_f}\right]^{m_f}}\right]\right]^p + k_{min}$$ [3]

where, k_s and k_{min} are saturated and minimum hydraulic conductivities, respectively; and p is the modified Campbell parameter.

3.2 Soil-atmosphere Model

The transient moisture flow through porous media was described according to the following equation (Wilson, 1997):

$$\frac{\partial}{\partial x}\left[\left(k_x^w + k^{vd}\right)\frac{\partial h}{\partial y}\right] + \frac{\partial}{\partial y}\left[\left(k_y^w + k^{vd}\right)\frac{\partial h}{\partial y} - k^{vd}\right] = -\gamma_w m_2^w \frac{\partial h}{\partial t}$$ [4]

Surface conditions needed to be identified to solve the governing equations. The following modified Penmen method was used to transform climate data into infiltration and evaporation fluxes at the soil surface for calculating potential evaporation (*PE*) per unit time, m/day (Gitirana, 2006):

$$PE = \frac{\Delta Q_N + E_a \gamma}{\Delta + \gamma}$$ [5]

where, Δ is slope of the saturation vapour pressure curve with respect to temperature (mmHg/$^\circ$F); Q_N is heat budget (m/day); γ is psychrometer constant (0.27 mm Hg/$^\circ$F). $E_a = f(u)p_{vsat}^{air}(1-RH_a)$, where ($p_{vsat}^{air}$) is the vapour pressure of air above surface (mm Hg); U_a is the wind speed (m/day); and RH_a is the relative humidity of air, and $f(u) = 0.35 (1 + 0.15U_a)$.

A series of constants (a_o = 0.6283580754, a_1 = 0.041142732, a_2 = 0.0017217473, a_3 = 0.000174108, a_4 = 0.0000003985, and a_5 = 0.0000000022) and atmospheric air temperature data T_a, ($^\circ$C) were used to calculate Δ and p_{vsat}^{air} as follows:

$$\Delta = a_1 + 2a_2 T_a + 3a_3 T_a^2 + 4a_4 T_a^3 + 5a_5 T_a^4 + 6a_5 T_a^5$$ [6]

$$p_{vsat}^{air} = a_0 + a_1 T_a + a_2 T_a^2 + a_3 T_a^3 + a_4 T_a^4 + a_5 T_a^5 + a_6 T_a^6$$ [7]

Similarly, denoting reflection coefficient by r; short wave radiation by R_c (m/day) (given by 0.95 R_a (0.18 + 0.55 n/N)); solar radiation by R_a (MJ/m^2/day), sunshine ratio by n/N, and Boltzman's constant by σ (W/m^2/K^4), the heat budget was calculated as follows:

$$Q_N = (1-r)R_c - \sigma T_a^4 (0.56 - 0.092(p_{vsat}^{air})^{0.5})(0.10 + 0.90\,n/N)$$ [8]

From the potential evaporation, the actual evaporation AE (m/day) was calculated using the following limiting function in SVFlux (Wilson, 1997):

$$AE = PE\left(\frac{p_v - p_v^{air}}{p_{vsat} - p_v^{air}}\right) = PE\left(\frac{RH_s - \left(\frac{p_{vsat}^{air}}{p_{vsat}}\right)RH_a}{1 - \left(\frac{p_{vsat}^{air}}{p_{vsat}}\right)RH_a}\right)$$ [9]

where, p_v, p_v^{air}, and p_{vsat} are vapor pressures (kPa) of the material surface of air near ground, and under complete saturation, respectively; and RH_s and RH_a are relative humidity at the material surface and in the air, respectively.

3.3 Soil-displacement Model

The soil displacement behaviour relative to the change in atmospheric conditions was predicted by using the concept of two independent stress state variables: net normal stress, ($\sigma - u_a$) and matric suction, ($u_a - u_w$), where σ is net total stress, u_a is pore-air pressure, and u_w is pore-water pressure (Fredlund and Morgenstern, 1977). The two-dimensional soil displacement analysis required the elasticity parameters E and H. The volume change index C_s (from net normal stress plane) and C_m (from matric suction plane) were obtained from the consolidation curve, *SWCC*, and the shrinkage curve (Fredlund and Rahadjo, 1993). The elasticity parameters were calculated as follows (Vu and Fredlund, 2004):

$$E = \frac{4.605(1+\mu)(1-2\mu)(1+e_0)}{C_s}(\sigma - u_a)$$ [10]

$$H = \frac{4.605(1+\mu)(1+e_0)}{C_m}(u_a - u_w)$$ [11]

where, E is the elasticity parameter for the soil with respect to net normal stress; H is elasticity parameter for the soil with respect to matric suction; and μ is Poisson's ratio for the soil structure.

The soil displacement in vertical and horizontal directions was solved in accordance with the following governing equation relative to the soil suction change (Vu, 2003):

$$\frac{\partial}{\partial x}\left\{C\left[(1-\mu)\frac{\partial u}{\partial x} + \mu\frac{\partial v}{\partial y} - \frac{(1+\mu)}{H}(u_a - u_w)\right]\right\} + \frac{\partial}{\partial y}\left\{G(\frac{\partial v}{\partial x} + \frac{\partial u}{\partial y})\right\} = 0$$ [12]

$$\frac{\partial}{\partial x}\left\{G(\frac{\partial v}{\partial x} + \frac{\partial u}{\partial y})\right\} + \frac{\partial}{\partial y}\left\{C\left[\mu\frac{\partial u}{\partial x} + (1-\mu)\frac{\partial}{\partial y} - \frac{(1-\mu)}{H}(u_a - u_w)\right]\right\} + pg = 0$$ [13]

Where, p is density of soil, g is acceleration due to gravity,

$$C = \frac{E}{(1-2\mu)(1+\mu)}, \quad \text{and} \quad G = \frac{E}{2(1+\mu)}.$$

4 SITE DISCRIPTION AND MODEL INPUT

4.1 Site Description

The city of Regina is developed on high expansive clay. It is in a semi-arid climate zone and often experiences a long period of rainfall deficit in summer. Civil infrastructure buried in the soil such as water mains has frequently experienced severe distress. To understand the soil behaviour, instruments were installed in a street of the city having a history of high water main breakage rate. The details of the instrumentation site can be found in Azam et al. (2010).

As shown in Figure 2, the model geometry consisted of a 15 x 6 m rectangle shape with heterogeneous (Regina clay, elastic silt, and till) soils (Azam et al., 2010). Climate conditions applied at about a halt of the top boundary to mimic the investigated field condition that consisted of vegetated park area and asphalt-paved area. Zero water flux was applied at the bottom boundary to represent no ground water table at 15 m depth at the investigation site. Daily climate data from May 1, 2009 to April 30, 2010 was obtained from the Regina International Airport weather station (located about 3 km from the investigation site). The initial matric suction was estimated to be 1600 kPa for the top 3 m, 2000 kPa for the till layer, and 600 kPa for the layer between the top layer and the till based on the field suction data measured by Vu, et al. (2007). Field suction data were measured on undisturbed soil samples using Whatman no. 42 filter paper together with a calibration curve suggested by Leong et al (2002). In the soil-displacement model, free movement of soil in the vertical direction was allowed at the top boundary and the horizontal movements of both the left and right sides were fixed. The lower boundary was fixed in both directions. A general purpose partial differential equation solver, FlexPDE was used for the analysis.
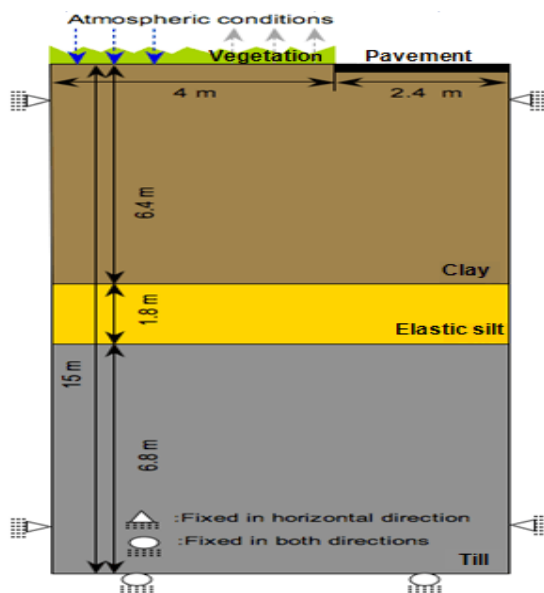

Figure 2. Model geometry and boundary conditions

4.2 Properties

Borehole drillings were made in July 2006 and May 2009 at Cross place, Regina, and the materials used for this numerical modelling had been investigated by Vu et al. (2007) and Azam et al. (2010), respectively. Figure 3 shows the grain size distribution curves for samples obtained in May 2009. The USCS classification is also presented in the legend and indicates that the soil consisted of several different layers. To avoid high complexity of numerical modelling, soil properties of a sample from 5.49 m depth were used to represent a clay layer in the model. The grain size distribution curve of a sample from 8.23 m depth was found to be a different material compared to the other curves thereby samples from 5.49 m and 8.23 m and till from the previous numerical study carried out by Vu et al. (2007) were selected for the material properties for this numerical modelling.

Figure 4 indicates the *SWCC* estimated for each soil used in this investigation and clearly shows how they contrasted. The sample from the 5.49 m depth of the till exhibited the gradation typical of fine-grained soils, whereas the gradation curve for the sample from the 8.23 m depth showed a sudden drop in the volumetric water content at lower suction range due to the presence of large pores.

Figure 5 shows the hydraulic conductivities as a function of soil suction. These curves well represented the pore-size distribution for each soil shown in the *SWCC* figure. The figure also indicated that the reduction in hydraulic conductivity occurred quickly for coarser materials and finer soils only started to deviate from the saturated hydraulic conductivity value at a suction around 100 kPa.

Soil properties used for the stress / deformation analysis are presented in Table 1. The elasticity parameter functions for the soil were calculated from the equation [10] and [11] by using the volume change indices and an assumed Poisson's ratio.

4.3 Climate Data

Figure 6 shows the climate data used for this numerical model. Figure 6a presents daily precipitation along with the cumulative values. The total precipitation was recorded to be 288 mm from May 1, 2009 to April 30, 2010. Rainfall primarily occurred during the summer months. During winter, the precipitation was received as snow. The cumulative snow precipitation was applied on a single day, when the temperature rose and remained above 0 °C in spring. Figure 6b shows the daily temperature. The annual mean temperature was found to be 2.7 ºC. The average from May to September was 14.4 ºC and the average from October to April was -5.8 ºC. The maximum difference between the high and low temperatures was 55.3 ºC. Relative humidity data and wind speed are shown in Figures 6c and 6d, respectively. The relative humidity data was generally inversely proportional to the temperature data. The average of relative humidity in winter was 78% and reduced to 64% in the summer. There was no clear trend for wind speed – it changed regardless of the season. The daily net radiation was estimated from the solar radiation measurement from November 1, 1999 to October 31, 2000 recorded in Swift Current, SK, by using albedo

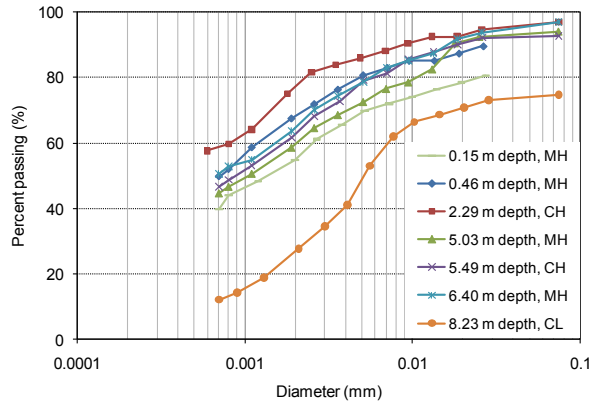values of 0.1 for the period from November 1 to March 31 and 0.3 for the rest of the year (Figure 6e).

Figure 3. Grain size distribution curve
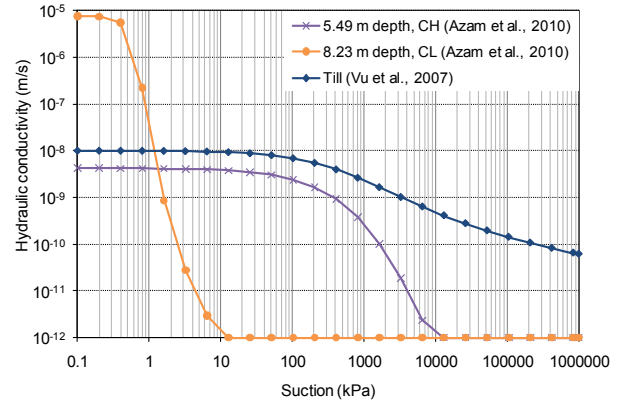
Figure 5. Hydraulic conductivity functions

Table1. Soil properties

Soil Property	Clay	Elastic Silt	Till
Dry unit weight[*1], γ_t (kN/m^3)	12.0	13.8	15.1
Initial void ratio[*1], e_0	1.2	0.9	0.7
Hydraulic conductivity[*2], k_{sat} (m/s)	9E-09	7.56E-06	10E-10
Saturated volumetric water content[*1] (%)	0.56	0.48	0.42
Swelling index[*1], C_s	0.09	0.09	0.09
Swelling index[*2], C_m	0.1	0.08	0.04
Poisson's ratio[*3], μ	0.33	0.3	0.3

[*1]: Derived from measured data
[*2]: Estimated from measured data
[*3]: Assumed value

Figure 4. Soil Water Characteristic Curve
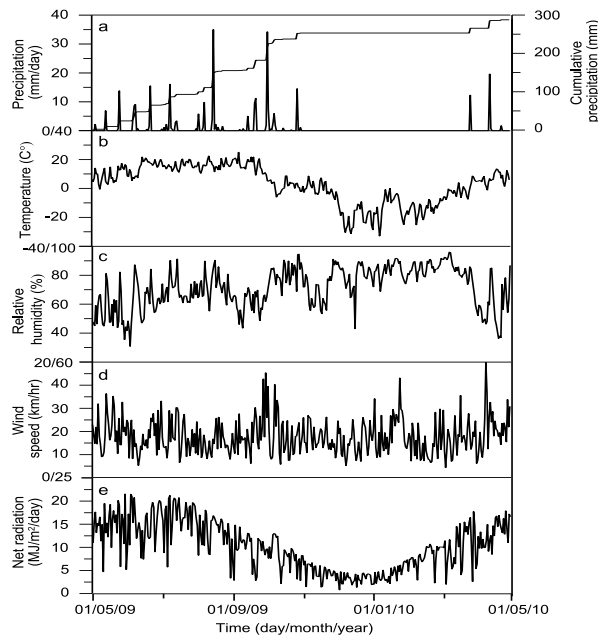
Figure 7 shows the cumulative boundary fluxes predicted for the "base case" model. Each flux can be distinguished into positive flux or negative flux. The total precipitation was 345 mm, comprised of 288 mm of natural precipitation and 57 mm of park watering. The predicted total net cumulative flux was predicted to be -25 mm. The total cumulative potential evaporation and actual evaporation were -417 mm and -401 mm, respectively.

Figure 8 and 9 highlight the fluctuation in the suction and volumetric water content at different depths during the modelling time period. Cyclical changes correlated well with the seasonal climatic conditions. The data obtained at the ground surface was found to fluctuate widely and these fluctuations gradually reduced with depth. The till layer showed minor variations corresponding to the change in atmospheric conditions on the boundary.

Figures 10 and 11 give the soil displacement history under the vegetated and pavement cover, respectively. The data was obtained at the centre point of each cover. Daily precipitation data are also presented in the plots. The upward soil displacements corresponded well with each precipitation event. The maximum daily swelling was predicted to be 4.0 mm and 0.7 mm at the ground surface under the vegetative and pavement cover, respectively.

Figure 6. Climate data
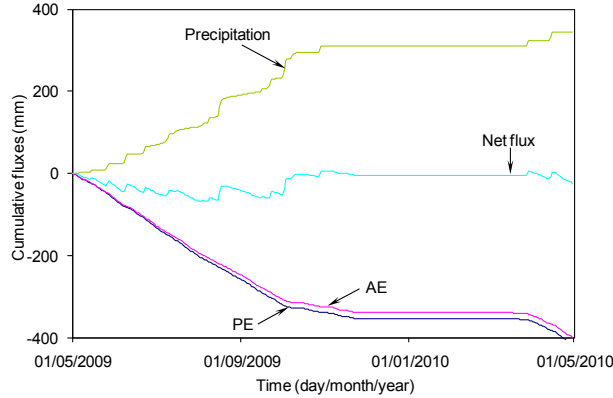
5   RESULTS AND DISCUSSIONS
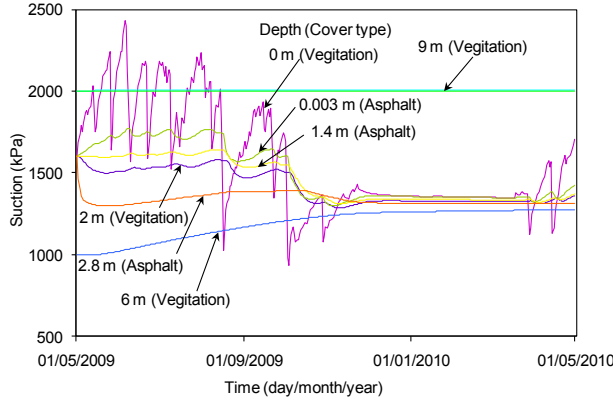
Figure 7. Cumulative fluxes
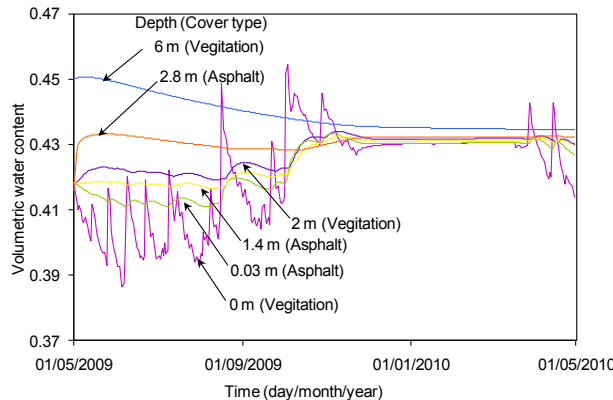

Figure 8. Suction history

Figure 9. Volumetric water content history

This means the surface exposed to atmospheric conditions was forecasted to have nearly 6 times more upward soil displacement compared to the pavement covered area. The fluctuation in the daily soil displacement ceased completely at a depth of around 6 m below the ground surface.

Figure 12 shows graphically the expected cumulative soil vertical displacement. (The vertical direction of the graphic is multiplied by 50 times to emphasize the volume changes.) The maximum volume stands for the largest soil volume increase achieved by the accumulation of daily soil displacements, whereas the minimum represents the smallest volume reached by the accumulation of daily soil displacements. The figure clearly indicates the cyclical soil movements and that the soil responded very well to the applied climatic conditions.

The difference between the maximum and minimum was found to be 13 mm for the base case model.
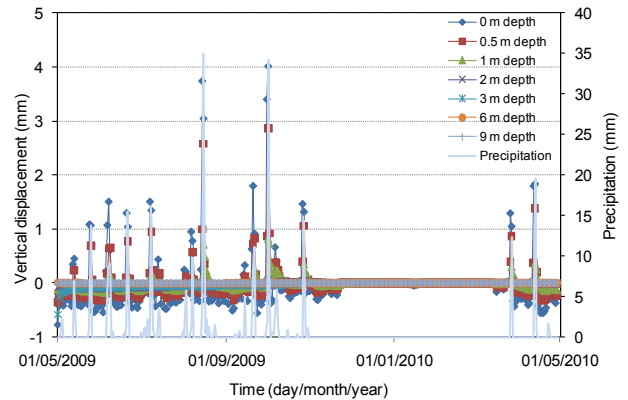

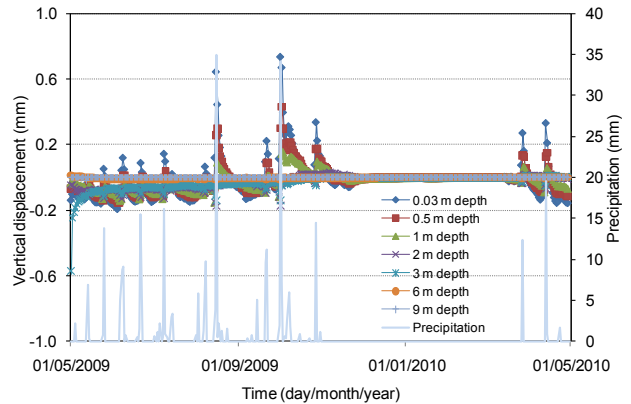Figure 10. Soil displacement under vegetative cover
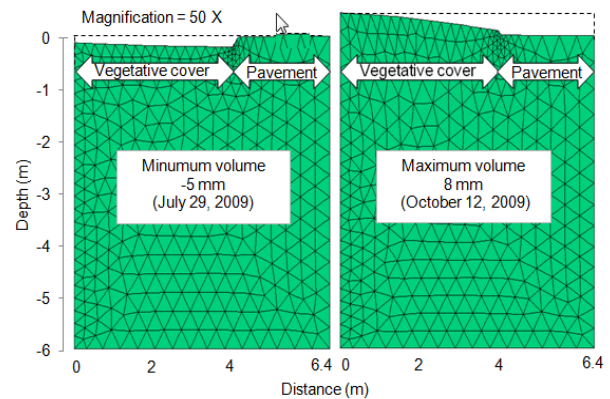

Figure 11. Soil displacement under asphalt cover

Figure12. Predicted minimum and maximum soil displacement

Figure 13 and 14 summarize the influence of each factor used in the parametric study performed on the soil-atmosphere model. There were clear trends that an increase in wind speed and net radiation factors lead to an increased negative net flux whereas an increase in precipitation and park watering factors leads to increased positive net flux. Maximum matric suction values were inversely proportional to the trend seen in the results for the net flux.
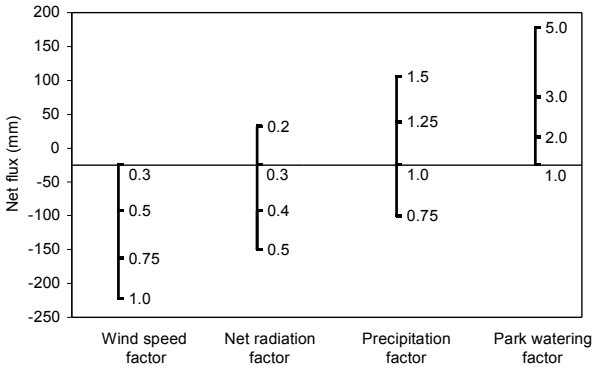
Figure 13. Net flux variations for climatic factors change at the vegetated ground surface
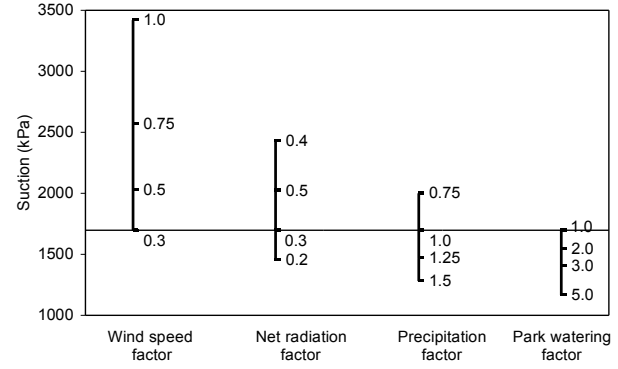

Figure 14 Suction variations for climatic factor changes at the vegetated ground surface

Table 2 gives the results from the parametric study carried out for the stress-displacement model. The atmospheric factors were necessary to output matric suction transfer files in the moisture flow model. A unique set of matric suction files existed for each parameter variation to be entered into the stress-displacement model. The additional soil property related factors such as the swelling index, the initial void ratio, and the Poisson's ratio were changed directly in the stress-displacement model. The greatest difference in annual soil volume was obtained by the subtraction of the minimum values from the maximum values. The maximum vertical displacement and the minimum vertical displacement were 8 mm and -5 mm, respectively for the base case model. From this, it was learned that maximum soil displacement was more sensitive to changes in atmospheric values. The largest vertical soil movement was predicted when 5 times more park watering was applied to the model. This resulted in 38 mm of upward shift, which is nearly 5 times more than the value found in the base case (8 mm).

Figure 15 shows the maximum difference in the cumulative vertical displacement predicted at the ground surface beneath the vegetative cover for the atmospheric factors. Both maximum and minimum vertical displacements increased or decreased linearly within each factor variation.

While increases in wind speed and net radiation decreased both maximum and minimum vertical displacements, the precipitation and park watering factor showed the opposite trend.

Since there was no vertical stress applied at the ground surface, the downward displacement occurring at the ground surface was considered to be caused by the shrinkage behaviour of the soil, which was encouraged by an increase in wind speed and net radiation. To the contrary, the upward displacement, which represents swelling, was dictated by an increase in precipitation and park watering. The park-watering factor was found to have a greater influence on the maximum soil displacement among the selected range of factor modifications.

Figure 16 gives the maximum difference in the cumulative vertical displacements predicted at the ground surface covered by vegetation with changing soil property factors. Like the results from weather-related factors, the fluctuation trend in the maximum and minimum soil displacement contrasted each other linearly for the swelling index and initial void ratio factors. The changes in the Poisson's ratio affected the minimum values inversely proportional manner, but somewhat there was no clear trend found for the maximum values. The swelling index was found to have more control on the variations in the degree of soil movement, the magnitude of the overall soil displacement was less severe compared to the displacements predicted due to atmospheric factor changes.

Table 2: Results from the parametric study for the stress/displacement model

| Parameter	Base case value	Value range	Maximum vertical displacement (mm)	Minimum vertical displacement (mm)	Annual maximum difference (mm)
Wind speed scale factor	0.3	0.5 to 1.0	1.5 to -7.6	- 6.0 to -9.7	7.4 to 2.0
Net radiation scale factor	0.3	0.2 to 0.5	-3.6 to 10.0	-9.0 to -2.2	5.4 to 12.3
Precipitation scale factor	1	0.75 to 1.5	-0.9 to 18.0	-5.8 to -2.0	4.9 to 20.0
Park watering factor	1	1 to 5	13.0 to 38.4	-2.0 to 5.6	15.0 to 32.8
Swelling index factor, C_m	0.09	0.07 to 0.14	3.6 to 8.4	-3.0 to -7.0	6.6 to 15.3
Initial void ratio factor, e_0	1.0	0.6 to 1.2	6.7 to 4.9	-5.6 to -4.1	12.3 to 8.6
Poisson's ratio factor, μ	0.33	0.2 to 0.45	4.6 to 4.9	-4.0 to -5.1	8.6 to 10.0
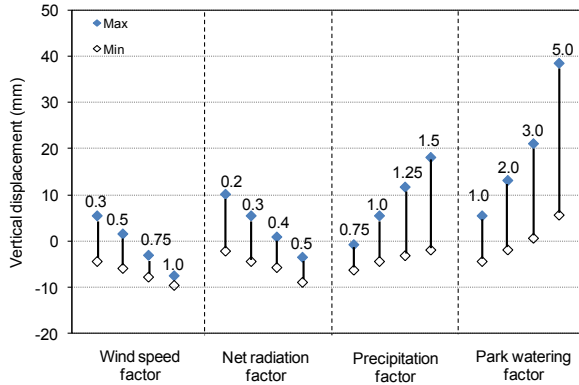
Figure 15. Soil displacement variations for changes in climatic factors at the vegetated ground surface
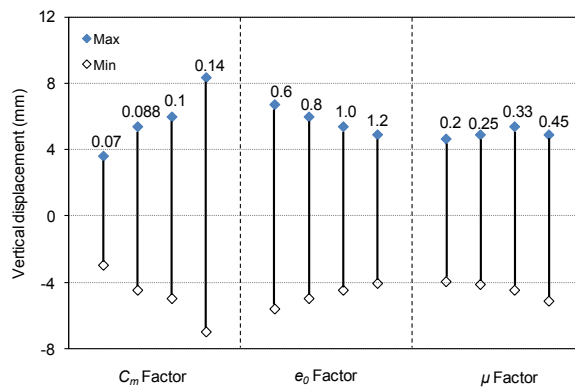

Figure 16. Soil displacement variations for change in soil property factors at the vegetated ground surface

6   SUMMARY

The unsaturated expansive soil behaviour was predicted through a combination of the soil-atmospheric and the soil-displacement models. The main conclusions can be summarized as follows:

1. Suction and volumetric water content data obtained at the ground surface was found to fluctuate widely and these fluctuations gradually reduced with depth.
2. The maximum daily swelling for the base case was predicted to be 4.0 mm and 0.7 mm at the ground surface under the vegetative and asphalt cover, respectively.
3. The accumulative minimum and maximum soil displacements were predicted to be -5 mm and 8 mm, respectively.
4. The precipitation, wind speed, and net radiation were found to significantly influence the changes in soil suction and thereby, the soil displacement.

REFERENCES

Azam, S., Ito, M. and Shah, I. 2010. *Behaviour of Asbestos Cement Water Mains in Expansive Soils*. Technical report to Communities of Tomorrow, Regina, SK.

Fredlund D.G. and Morgenstern, N.R. 1977. Stress State Variables for Unsaturated Soils. *ASCE Journal of Geotechnical Engineering*, 103: 447-466.

Fredlund, D.G. and Rahardjo, H. 1993. Soil Mechanics for Unsaturated Soil. John Wiley & Sons, New York.

Fredlund, D.G. and Xing, A. 1994. Equation for the Soil-Water Characteristics Curve. *Canadian Geotechnical Journal*, 31: 521-532.

Fredlund, M.D. 2004, *SoilVision Theory Manual*. SoilVision Systems Ltd., Saskatoon, SK.

Fredlund, M.D., Wilson, G.W. and Fredlund, D.G. 2002. Use of the Grain-size Distribution for Estimation of the Soil-water Characteristic Curve. *Canadian Geotechnical Journal*, 39: 1103-1117.

Gitrana, G. Jr., Fredlund, M.D. and Fredlund, D.G. 2006. Numerical Modeling of Soil-atmosphere Interaction for Unsaturated Surfaces. *4th International Conference on Unsaturated Soils*, Carefree, AZ, USA, 1-12.

Leong, EC, He, L. and Rahardjo, H. 2002. Factors affecting the filter paper method for total and matric suction measurements. *Geotechnical Testing Journal*, ASTM International, 25(3): 322-333.

Penman, H.L. 1948. Natural Evaporation from Open Water, Bare Soil, and Grass. *Proceedings of the Royal Society A.,* London, 193:120-145.

Vu, H.Q. 2003. *Uncoupled and Coupled Solutions of Volume Change Problems in Expansive Soils*. Ph.D. thesis, Department of Civil Engineering, University of Saskatchewan, Saskatoon, SK.

Vu, H.Q. and Fredlund D.G. 2004. The Prediction of One-Two-, and Three-dimensional Heave in Expansive Soils. *Canadian Geotechnical Journal*, 41: 713-737.

Vu. H. Q., Hu, Y. and Fredlund, D.G. 2007. Analysis of Soil Suction Changes in Expansive Regina Clay, *Proceedings. 60th Canadian Geotechnical Conference*, Ottawa, ON, Canada, 1069-1076.

Wilson, G.W., Fredlund, D.G. and Barbour, S.L. 1994. Coupled Soil Atmosphere Modeling for Soil Evaporation. *Canadian Geotechnical Journal,* 31: 151-161.

Wilson, G.W., Fredlund, D.G. and Barbour, S.L. 1997. The Effect of Soil Suction on Evaporative Fluxes from Soil Surfaces. *Canadian Geotechnical Journal*, 34: 145-155.

Wilson, G.W. 1997. *Surface Flux Boundary Modeling for Unsaturated Soils*. Unsaturated Soil Engineering Practice, Geotechnical Special Publication No. 68, Houston, S.L. and Fredlund, D.G., ed., ASCE, 38-65.